Ultrasonic Phased-Array Three-Dimensional Imaging Detection for Insulation Component Positions in Ultra-High Voltage Transformers

Junli Du[1,*], Chao Li[1], Chaohua Wang[1], Yongfeng Zhao[1], Hua Zhu[1], Rui Qiu[2], Guanhua Wu[2], Xi Chen[2]

[1]State Grid Henan Electric Power Company Power Science Research Institute, Zhengzhou, Henan 450052, China
[2]Key Laboratory of Non-Destructive Testing Technology (Nanchang Hangkong University), Nanchang, Jiangxi 330063, China

*Corresponding author: dujunlizz@163.com

Abstract. To accurately detect the position of the paper insulating component inside the UHV (ultra-high voltage) transformers and prevent the discharge fault, the research on ultrasonic phased array three-dimensional imaging detection technology of the insulating cardboard position was carried out. Firstly, a large-size multi-medium (steel-oil-paper-steel) simulation detection component was fabricated, and a multilayer medium accurate positioning method based on sound velocity error compensation was established. Based on Snell's theorem, the focused delay rule of the ultrasonic phased array in a multilayer medium is established, and the effectiveness of the focus delay rule is verified in the finite element simulation model of acoustic propagation in a multilayer medium. According to the characteristics of the data collected by phased array ultrasonic testing, combined with the structure of the transformer bushing, the point cloud data with three-dimensional spatial coordinates and characteristic values is generated to realize the three-dimensional visual imaging of the detection results. The results show that the established ultrasonic phased array three-dimensional imaging detection method can effectively realize the positioning detection and three-dimensional imaging of the position of the insulating cardboard in the bushing, providing advanced nondestructive testing technology for ensuring the safe operation of the UHV/EHV transformer.

Keywords: Ultra-high voltage transformer; insulation component; position detection; three-dimensional imaging; phased array ultrasonic inspection

1 Introduction

Partial discharge occurs in the insulation components of critical parts of ultra-high voltage transformers, causing a complete breakdown of the insulation layer and leading to accidents such as fires, equipment burns, and equipment shutdowns, seriously affecting the safety of ultra-high voltage power grids. The investigation and analysis indicate[1-5]

H. Bilgin et al. (eds.), *Proceedings of the 2024 6th International Conference on Civil Engineering, Environment Resources and Energy Materials (CCESEM 2024)*, Advances in Engineering Research 253,
https://doi.org/10.2991/978-94-6463-606-2_5

that the cause of the accident was the displacement of the insulation cardboard inside essential connection parts, such as transformer bushing and transformer riser, which led to discharge faults. The transformer bushing is cylindrical, about 500 mm~1000 mm in diameter, and the outer steel plate is 10 mm~20 mm thick. The internal centre is the transmission component, and transformer oil is the filling medium between the outer and central parts. One or more layers of cylindrical insulation cardboard are placed around the central internal component in the transformer oil. Due to the natural circulation of transformer oil expansion and contraction inside the bushing, it belongs to a semi-dead oil zone" state. When the position of the insulation cardboard in this area is offset, discharge breakdown accidents are prone.

Detecting partial discharge in the live state of ultra-high voltage equipment[6] usually uses chemical detection, high-frequency current method, acoustic emission method, ultrasonic method, ultra-high frequency method and other detection methods[6-12]. Among them, the ultrasonic method detects the release of heat energy during partial point discharge, and the insulation medium expands due to heat. After the discharge, the medium returns to its original volume and generates ultrasonic waves. The high-frequency current method involves winding multiple turns of metal conductive coils around a ring-shaped magnetic core to form a sensor installed on the ground wire of power equipment. When partial discharge occurs, the pulse current inside the power cable or equipment will be conducted to the ground through the ground wire. At this time, the high-frequency current sensor will generate induced voltage to detect the amount of partial discharge[13]. The acoustic emission method[14-15] detects partial discharge by monitoring the signal changes of ultrasonic waves propagating inside the transformer oil tank. However, long-term built-in acoustic emission sensors are required for detection. Considering that the displacement of insulation cardboard is one of the leading causes of partial discharge faults if the position of insulation cardboard can be regularly detected, the displacement situation can be detected promptly. The status monitoring of the insulation cardboard position can be achieved, effectively preventing discharge faults and ensuring the safe operation of equipment. The existing transformer condition monitoring technology is limited, and the monitoring timing needs to catch up. A new detection method is needed to provide early warning before partial discharge faults occur[16].

The position detection of insulation cardboard in ultra-high voltage equipment belongs to the positioning detection of large-sized (100mm-400mm) multi-media, requiring a detection method with solid penetration and a high detection rate for area-type defects. Ultrasonic testing technology[17] has strong penetration ability and is suitable for detecting the position of insulation cardboard in ultra-high voltage equipment. Ultrasonic phased array detection technology[18] has flexible and controllable sound beams suitable for complex and rapid structure detection. However, due to the smaller size of the array elements in the sensor compared to the crystal size in conventional ultrasonic probes, conventional industrial ultrasonic phased array detection technology makes it challenging to meet the needs of insulation paperboard position detection in ultra-high voltage equipment in terms of sound field intensity and sound beam penetration ability. More ultrasonic phased array detection and imaging methods are needed for insulation paperboard in ultra-high voltage equipment regarding parameter setting, analysis, and evaluation of detection results.

Research on ultrasonic positioning detection and 3D imaging technology for detecting the position of insulation cardboard in ultra-high voltage equipment. A sound velocity compensation method is established by analyzing the influence of different grades and temperatures of transformer oil on ultrasonic sound velocity positioning. Design an ultrasonic phased array focusing method suitable for insulation paperboard of ultra-high voltage equipment, convert the detection results into coordinates, generate point cloud data, and perform 3D imaging to achieve precise positioning and 3D position visualization of insulation paperboard. This is significant for improving the detection accuracy of ultra-high voltage equipment and realizing the warning function for partial discharge.

2 Theory Analysis

2.1 Phased Array Ultrasonic Focusing Method for Large-Sized Multi-Media

Taking four layers of media as an example, sound waves need to pass through four different media for focused detection. According to Snell's law, when sound waves are incident on the interface between two media at a certain angle, they will undergo reflection and refraction phenomena at the interface. When using the ultrasonic phased array detection method to detect the bushing device of ultra-high voltage equipment to ensure the sound field intensity and penetration depth, the theoretical sound path distribution of all array elements focused is shown in Figure 1.

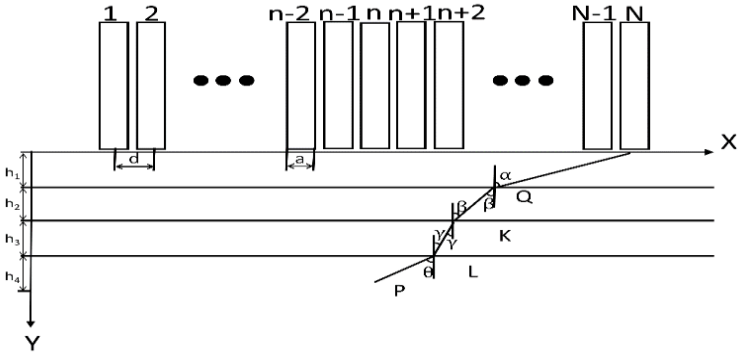

Fig. 1. Focused acoustic paths of ultrasonic phased array elements in four-layer media

Assuming the thickness of the first layer of medium is h_1, the thickness of the second layer of medium is h_2, and the thickness of the third layer of medium is h_3, the incident angle of the sound wave generated by any element of the array $n(n = 1,2,3, \dots, N)$ is α, the refractive angle the first layer of the medium and the incident angle of the second layer of medium are β, the incident angle of the second layer of medium and the refractive angle of the third layer of medium is γ , the refractive angle of the fourth layer of medium is θ , the refractive point and coordinates are $\mathrm{Q}(x_Q, y_Q)$, $\mathrm{K}(x_K, y_{QK})$, $\mathrm{L}(x_L, y_L)$ and the focal point is reached $\mathrm{P}(x_P, y_P)$. The coordinate of the element is $(x_n, 0)$, and can be obtained from Snell's law and Pythagorean theory:

$$\frac{sin\alpha}{c_1} = \frac{sin\beta}{c_2} = \frac{sin\gamma}{c_3} = \frac{sin\theta}{c_4} \tag{1}$$

$$sin\alpha = \frac{|x_N - x_Q|}{\sqrt{(x_N - x_Q)^2 + h_1^2}} \tag{2}$$

$$sin\beta = \frac{|x_Q - x_K|}{\sqrt{(x_Q - x_K)^2 + h_2^2}} \tag{3}$$

$$sin\gamma = \frac{|x_K - x_L|}{\sqrt{(x_K - x_L)^2 + h_3^2}} \tag{4}$$

$$sin\theta = \frac{|x_Q - x_P|}{\sqrt{(x_Q - x_P)^2 + (y_P - h_1 - h_2 - h_3)^2}} \tag{5}$$

$$|x_N - x_P| = sin\alpha + sin\beta + sin\gamma + sin\theta \tag{6}$$

$$t_n = t_{max} - \left(\frac{\sqrt{(x_N - x_Q)^2 + h_1^2}}{c_{31}} + \frac{\sqrt{(x_Q - x_K)^2 + h_2^2}}{c_2} + \frac{\sqrt{(x_K - x_L)^2 + h_3^2}}{c_3} + \frac{\sqrt{(x_Q - x_P)^2 + (y_P - h_1 - h_2 - h_3)^2}}{c_4} \right) \tag{7}$$

From equation (1) to equation (6), the horizontal coordinates of the refractive points Q, K, and L can be solved. Substituting them into equation (7), the delay time of the excitation sound waves for each array element can be obtained, which is the phased array ultrasonic focusing law for large-sized multi-media.

Various acoustic problems in engineering calculation models can be described through wave equations and boundary conditions. When the boundary conditions are set correctly, the unique correct solution to the wave equation can be solved. For isotropic media with elastic coefficients, the wave equation (8) is:

$$(\lambda + 2\mu)\nabla\nabla u - \mu\nabla \times \nabla \times u = \rho \frac{\partial^2 u^2}{\partial t^2} \tag{8}$$

in which λ and μ is Lame coefficient, u is particle displacement, and ρ is object density.

When ultrasound propagates, the stress changes in the same direction of the tested object of the same gender are consistent. To reduce computational complexity and analyze the internal sound field of the tested object, a two-dimensional cross-sectional model is used as the simulation model. A multi-layer dielectric simulation model with a width of 50 mm (Figure 2) is established by Comsol finite element software, in which a 5mm wide absorption layers on both sides of the model is also added to absorb and diffuse ultrasonic waves. The first and fifth layers are made of structural steel with a medium of 5900m/s, the second and fourth layers are made of transformer oil with a medium of 1400m/s, and the third layer is made of cardboard with a medium of

2200m/s. The thickness from the first layer to the fifth layer is 3mm, 10mm, 5mm, 15mm, and 3mm, respectively. Set up 16 array elements on the upper interface of the first layer medium, with a width of 1mm and a spacing of 0.02 mm.

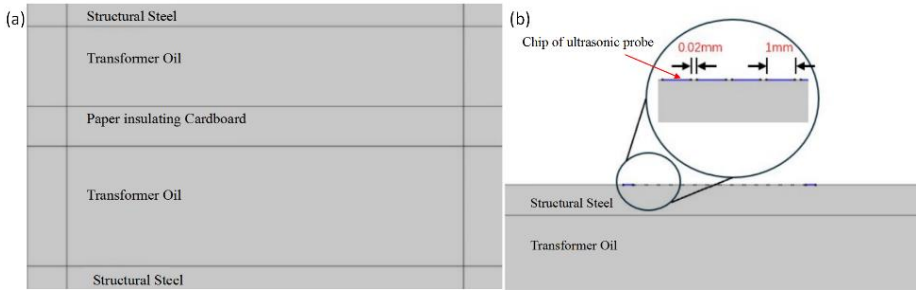

Fig. 2. Multi-layer medium acoustic simulation model. (a) five layer medium acoustic simulation model; (b)the location of chip of ultrasonic probe in simulation model.

Considering the use of multiple layers of insulating cardboard in actual components, in order to simulate the sound wave penetrating the first layer of insulating cardboard and focusing on the surface of the second layer of insulating cardboard, the focusing point is set at the centre of the fourth layer medium at a depth of 10mm. Based on the model parameters, the delay time of each array element exciting the sound wave is calculated and simulated. The simulation results of the sound field model with and without focus are shown in Figure 3.

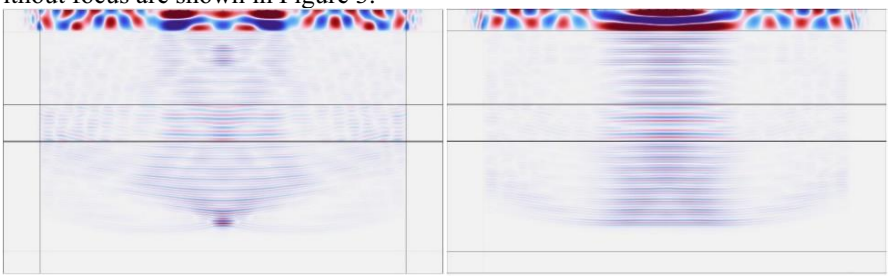

Fig. 3. Simulation validation for focusing law of ultrasonic phased array detection. (a) Focusing; (b) Unfocusing.

By comparing the variation curve of the probe points set in the fourth layer medium (Figure 4), it can be concluded that the ultrasonic sound pressure obtained through delayed focusing is about twice that of the ultrasonic sound pressure obtained without focusing. It can be seen that the calculated multi-layer dielectric phased array ultrasonic delay focusing method can achieve the gathering of sound beams in the insulating cardboard area, improve the sound field intensity, enhance the accuracy in multi-layer dielectric ultrasonic testing, and significantly improve the lateral accuracy of the sound field and the amplitude of the echo sound pressure at the focusing point.

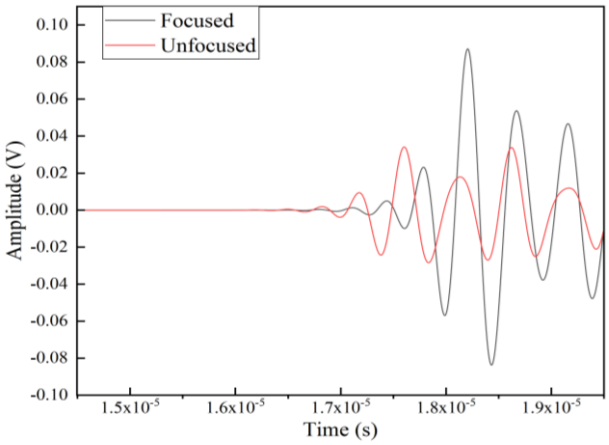

Fig. 4. Sound pressure distribution at focused position

2.2 Large Scale Multi-Media Phased Array Ultrasound 3D Imaging Method

The bushing of ultra-high voltage transformers is mostly made of curved workpieces. When testing based on existing ultrasonic phased array equipment, due to the limitations of instrument functions, the exported data files do not have the characteristics of fan scanning angles and the coordinate characteristics of curved surfaces. Therefore, directly imaging them is a rectangular shape in the Cartesian coordinate system, which needs to be converted into a cylindrical coordinate system and reassigned with fan scanning angles, as shown in Figure 5.

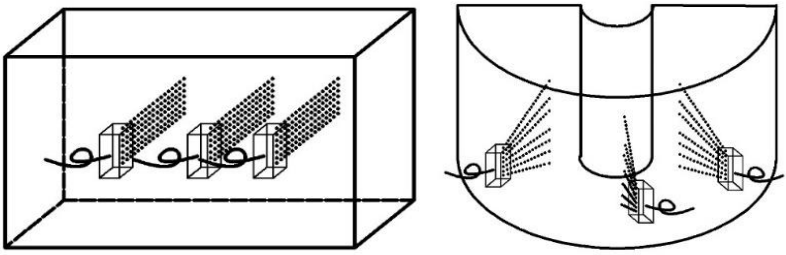

Fig. 5. Spatial position distribution of point clouds for ultrasonic phased array inspection data of curved work pieces. (a) Phase array device original point cloud; (b) Point cloud after coordinate conversion.

The calculation of coordinate transformation needs to be divided into two parts. Firstly, the sector scanning data exported from the phased array board that does not have angle values should be reassigned with corresponding angle values. Assuming the sound velocity of the first layer medium is C_1, the sound velocity of the second layer medium is C_2, and the incident angle is θ, according to Snell's theorem, the angle α after refraction can be calculated by equation (9):

$$\alpha = sin^{-1}(\frac{C_2 \times sin\theta}{C_1}) \tag{9}$$

If the sector scanning angle range in the ultrasonic phased array board sets as -30°~30° and the angle interval is 1°, then the angle calculation formula (10) is:

$$\alpha_i = sin^{-1}(\frac{C_2 \times sin\theta_i}{C_1}) \tag{10}$$

in which θ_i is the ith incident angle, α_i is the ith refractive angle.

The discrete digital A-scan signal of the first sector scanning incident angle, assuming the unit distance between each discrete point is j, and the coordinate of the first point is (x_j, y_j), the coordinate of the first point can be calculated by equation (11).

$$\begin{cases} x_j = j \times cos\alpha_1 \\ y_j = j \times sin\alpha_1 \end{cases} \tag{11}$$

The coordinate of the ith incident angle and the nth point can be calculated by equation (12).

$$\begin{cases} x_{nj} = n \times j \times cos\alpha_i \\ y_{nj} = n \times j \times sin\alpha_i \end{cases} \tag{12}$$

Considering that the actual detection object is a curved work-piece, converting the ultrasonic phased array detection results displayed in the Cartesian coordinate system to a cylindrical coordinate system. If the arc length for moving the surface by one unit is k, then the rotation angle of one arc length step can be calculated by formula (13).

$$\beta = \frac{k \times 180}{\pi R} \tag{13}$$

in which R is the radius of the inspected curve. Therefore, the angle of the m^{th} unit arc length can be calculated by formula (14).

$$\beta m = m \times k \times 180 \pi R \tag{14}$$

Starting from the origin of the coordinate system with the center of the circle, assuming the Z-axis coordinate is 0, without considering the assignment of sector scanning coordinate, the unit distance between discrete points is also j. After scanning the m^{th} unit arc length on the surface, the coordinate of the n^{th} point can be calculated by formula (15).

$$\begin{cases} x_{nj} = (\mathrm{R} - n \times j) \times sin\beta_m \\ y_{nj} = (\mathrm{R} - n \times j) \times cos\beta_m \\ z = 0 \end{cases} \tag{15}$$

Therefore, the steps for three-dimensional coordinate reconstruction are as follows: (1) Establishing a cylindrical coordinate system, with both the positive Y-axis and XZ axis as 0 points, the surface of the cylinder as the initial position, the OXY plane per-

pendicular to the direction of the array element arrangement, and the OYZ plane parallel to the initial position and array element arrangement. The complete coordinate system is shown in Figure 6.

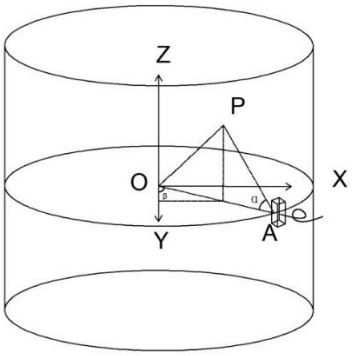

Fig. 6. Three-dimensional cylindrical coordinate system

The deflection angle after sector scanning refraction is α, the rotation angle of the surface is β, the radius of the cylinder is R, the distance between point P and point A where the probe located is the nth unit distance j. Therefore, the three-dimensional coordinate of point P in Figure 3 can be calculated by equation (16).

$$\begin{cases} x_P = (\mathrm{R} - n \times j \times cos\alpha_P) \times sin\beta_P \\ y_P = (\mathrm{R} - n \times j \times cos\alpha_P) \times cos\beta_P \\ z_P = n \times j \times sin\alpha_P \end{cases} \tag{16}$$

3 Experimental Confirmation

Based on the structure and dimensions of the outlet device of the ultra-high voltage transformer, a multi-layer dielectric large-scale simulation sample of steel/oil/paper/steel is replicated, as shown in Figure 7.

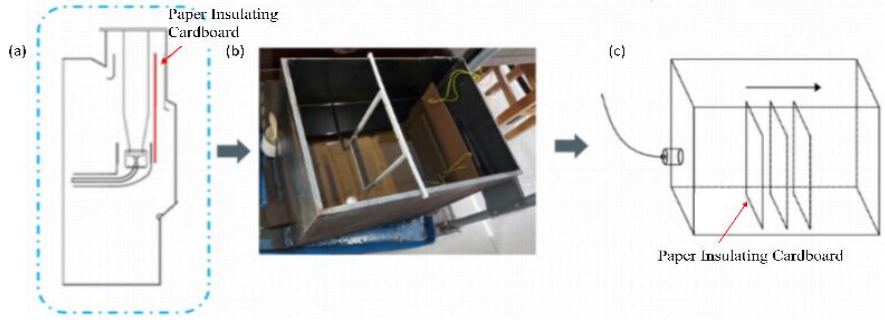

Fig. 7. Schematic diagram of simulated sample. (a) schematic diagram of the outlet device of ultra-high voltage transformer.(b) the experimental paper insulating cardborad of position detection by ultrasonic phased-array measurement; (c) the schematic diagram of measurement.

In order to improve the accuracy of positioning specific interfaces (oil/paper) in multi-layer medium detection, the positioning values in ultrasonic detection instruments are compensated and corrected. Assuming the sound velocity of the first layer medium is C_1, the sound velocity of the second layer medium is C_2, the sound path of the first layer medium is S_1, and the sound path from the interface between the first and second layers of medium to the reflector is S_2.

For the convenience of calculation and device display, the sound speed of the medium with a larger sound path is selected as primary parameters of the ultrasonic detection instrument. Setting $S_2 > S_1$, the input sound speed value is C_2. The total time T_t of the echo signal can be divided into two parts, including the propagation time T_1 of the first layer of medium and the time T_2 from the interface between the first layer of medium and the second layer of medium to the reflector. Thus, the sound path distance from instrument of echo signal S_i, the sound path distance error S_e, and the corrected sound path distance S_a can be calculated by formula (17), formula (18) and formula (19) respectively.

$$S_i = C_2 \times T_t = C_2 \times (T_1 + T_2) = C_2 \times T_1 + C_2 \times T_2 \tag{17}$$

$$S_e = (C_2 - C_1) \times T_1 = (C_2 - C_1) \times \frac{S_1}{C_1} \tag{18}$$

$$S_a = S_i - S_e = S_i - (C_2 - C_1) \times \frac{S_1}{C_1} \tag{19}$$

When the tested object is an N layer medium, taking the sound velocity C_i of the i layer （$i < N$） as the largest sound velocity of the medium, the actual sound path distance S_{aN} of the N layer medium can be calculated by formula (20).

$$S_{aN} = S_i - \sum_{j=1}^{n} (C_i - C_j) \times \frac{S_i}{C_j} \tag{20}$$

Using a simulated sample as the detection object, measure the distance between the probe and the insulating cardboard in the area of 100 mm~300 mm, with a 10 mm interval between each position. CTS-1010 digital ultrasound instrument is selected, and the probe model, frequency, and chip size are shown in Table 1. Adjust the equipment so that the echo wave height at 50 mm sound path is 80% of the full screen. Move the position of the insulation cardboard to make the distance from the probe 50 mm, 100 mm, 150 mm, 200 mm, 250 mm, 300 mm, and 350 mm at a time. Record the amplitude of the echo sound pressure, and the test data is shown in Figure 8.

Table 1. Probe parameters

probe model	frequency/MHz	chip size /mm
1P25	1	25
1P20	1	20
1P14	1	14
1.5P20	1.5	20
1.5P14	1.5	14
2P14	2	14
2.5P14	2.5	14

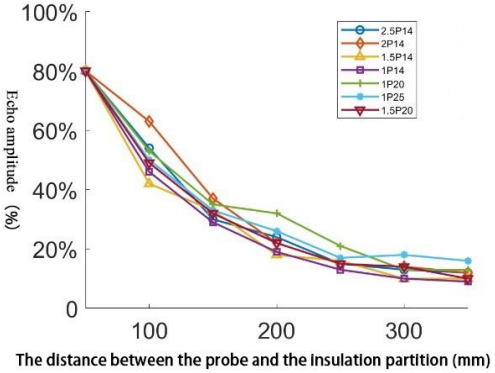

Fig. 8. Echo sound pressure at different insulation board positions

Analyzing the echo sound pressure of probes with different frequencies and chip sizes for detecting insulation cardboard at different positions, it was found that when the sound path distance was in the range of 50 150 mm, the higher the frequency and the smaller the chip size, the higher the detected echo sound pressure. Probe 2P14 was superior to other probes. In the range of 150 mm~350 mm, as the sound path increases, the 1P25 and 1P20 probes have higher frequencies and smaller chip sizes compared to other probes, and their echo sound pressure is more suitable for coordinate positioning.

The current temperature of the transformer oil is measured to be 24.8 ℃, and the sound velocity of the transformer oil is $C_{oil}^{24.8℃} = 1456.7 - 3.1275 \times 24.8 = 1379.138\, m/s$. By inputting the sound velocity of $1379.138\, m/s$ as the primary parameter, the positioning value of the paper insulation component can be obtained by instrument, as shown in Figure 9. The error of the position of paper insulation component using 7 different types of probes is about 5mm~10mm, with the maximum error percentage reaching about 9%.

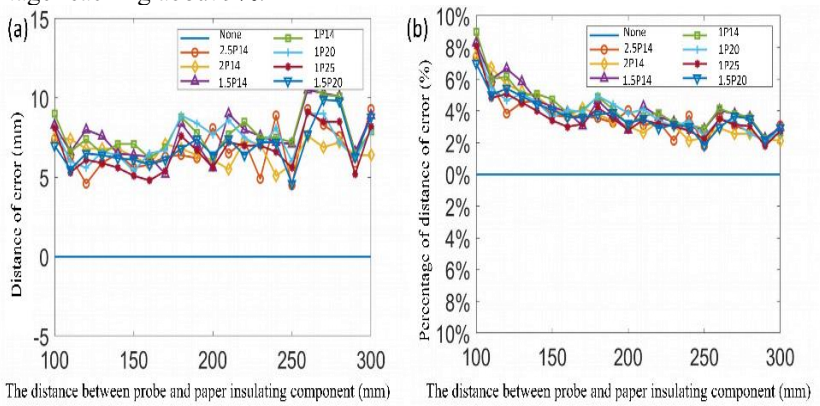

Fig. 9. Positioning errors of ultrasound instruments before velocity correction. (a) the position error; (b) the percentage of error.

The position error of all the data after acoustic path compensation is shown in Figure 10. The maximum error and the actual coordinate value is only 2.66 mm after correction, with a maximum error percentage of 2.5%, which enhanced obviously compared to original data.

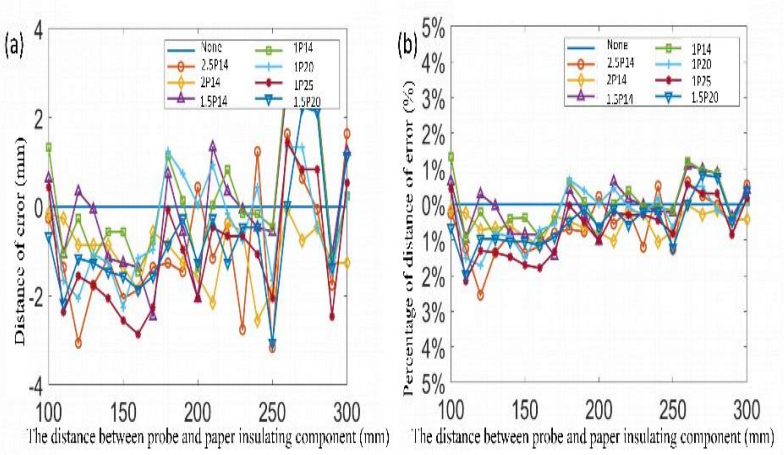

Fig. 10. Positioning errors of ultrasonic instruments after sound velocity correction. (a) the position error; (b) the percentage of error.

By combining the amplitude of point P in the ultrasonic phased array board, i.e. the intensity value I, point cloud data with four parameters XYZI can be established to generate point cloud data (PCD) files. Perform clutter reduction, amplitude filtering, and target enhancement on PCD point cloud data to increase the amplitude of multilayer media interface echoes for 3D imaging, as shown in Figure 11. The three-dimensional imaging of the insulation partition/oil interface after target enhancement is clearer, more accurate, and easier to identify.

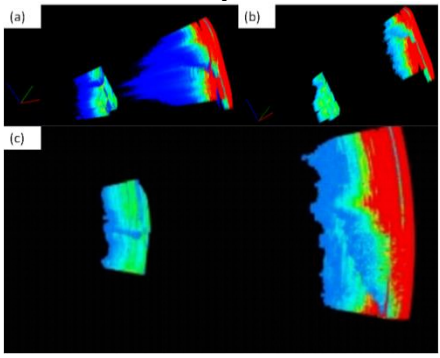

Fig. 11. Processing and 3D imaging of point cloud data. The color of the image respects the intensity of signal of paper insulator component. (a) before filtering; (b) after filtering; (c) after target enhancement.

4 Conclusion

An ultrasonic positioning detection method based on sound velocity compensation is proposed to meet the technical requirements for detecting the position of paper insulation components inside the bushing of ultra-high voltage transformers under work state. We designed an ultrasonic phased array detection focusing rule and simulated it by experimental verification, which is suitable for detecting the paper insulation component position. To address the issue of performing cylindrical coordinate 3D imaging by phased array equipment, we proposed the method with coordinate transformation and 3D imaging based on point cloud data. Finally, ultrasonic phased array positioning detection and 3D imaging of the internal insulation cardboard position of ultra-high voltage equipment sleeves and other equipment were achieved, with a positioning error within 1%.

Acknowledgment

This work is financially supported by the Science and technology project of State Grid Henan Electric Power Company(521702220001)

References

1. QING Song, LI Bin, ZHANG Dawei, et al. Detection and treatment of internal discharge defects of 220 kV transformer[J]. Shandong electric power Technology, 2018, 45(11):27-31.
2. ZHANG Kai, ZHANG Chengfei, DONG Honglin, et al. Analysis and treatment of 220kV transformer partial discharge fault[J]. Transformer, 2019, 56(10):48-51.
3. WANG Jiangwei, LI Jie, SHI Wei, el at. Analysis of trip fault of main transformer in 500 kV substation[J]. 2021, 48(1):22-26.
4. He Z , Zhao L J , Zhao Y ,et al. Dissolved gases generated of partial discharges and electrical breakdown in oil-paper insulation under AC-DC combined voltages[J].IEEE, 2012. DOI:10.1109/ICHVE.2012.6357116.
5. Ma Z , Cheng Y , Chen M ,et al. Study on the influence of gases on white marks and carbonized tracks generated by partial discharge in transformer oil-paper insulation[J]. IEEE, 2013. DOI:10.1109/ICSD.2013.6619886.
6. Islam M M, Lee G, Hettiwatte S N. A review of condition monitoring techniques and diagnostic tests for lifetime estimation of power transformers[J]. Electrical Engineering, 2018, 100(4): 581-605.
7. YI Feng, LIANG Jian, XU Wei. et al. Abnormal analysis of partial discharge in 500 kV transformer[J]. Shandong electric power Technology, 2020, 47(08):10-13.
8. FENG Xiaoze, KOU Peng, LIANG Deliang, et al. Spatial localization method of transformer partial discharge based on compressive sensing and fingerprint[J]. High voltage electrical apparatus.2023, 59(12):160-167.
9. Guo Jiayuan, Li Chengzhen, Zhao Tingzhi, et al. Diagnosis and analysis of internal discharge in 500 kv transformer based on joint positioning method[J]. Sichuan electric power technology. 2024, 1:105-110.

10. Zhang X R, Shi M X, Cai J, et al. A novel partial discharge detection method for power transformers on site adopting its component as ultra-high frequency sensor [J]. IEEE Transactions on Power Delivery, 2019, 34(6): 2269-2271.
11. Razzaq A, Zainuddin H, Hanaffi F, et al. Transformer oil diagnostic by using an optical fibre system: a review [J]. IET Science Measurement & Technology, 2019, 13(5): 615-621.
12. Zachariades C, Shuttleworth R, Giussani R, et al. Optimization of a high-frequency current transformer sensor for partial discharge detection using finite-element analysis [J]. IEEE Sensor Journal, 2016, 16(20): 7526-7533.
13. MA Lifei. Study on the characteristics of high frequency current sensor for partial discharge detection[D]. Dalian:Dalian Jiaotong University, 2022.
14. Danijel B, Dalibor F. Improvement of ultrasonic method for testing of power transformers[J]. Procedia Engineering, 2017, 202(9):189-201.
15. Kunicki M, Wotzka D. A Classification Method for Select Defects in Power Transformers Based on the Acoustic Signals[J]. Sensors. 2019, 19(23):5212.
16. Rahul S, Bhinal M. Review on asset management of power transformer by diagnosing incipient faults and faults identification using various testing methodologies[J]. Engineering Failure Analysis, 2021, 128(10): 105634.
17. Sandeep K D, Manish V, Akhilesh S. Advances and Researches on Non Destructive Testing: A Review[J]. Materials Today: Proceedings, 2018, 5(2): 3690-3698.
18. ZHANG Penghui, ZHAO Yang, LI Peng, et al. Research Progress in Ultrasonic Imaging Detection Technology[J]. Laser & optoelectronics progress, 2022, 59(2): 0200003.